Wear 494–495 (2022) 204247

Contents lists available at ScienceDirect

Wear

journal homepage: www.elsevier.com/locate/wear

Correlating nano-tribological behavior with the free volume of Zr-based bulk metallic glasses via their fictive temperature

Wanfu Dong [a,1], Jianping Lai [a,1], Jiaxin Yu [a,*], Udo D. Schwarz [b,c], Yifan Zhang [a], Kun Zhu [a], Amit Datye [b,**]

[a] Key Laboratory of Testing Technology for Manufacturing Process in Ministry of Education, State Key Laboratory of Environment-friendly Energy Materials, Southwest University of Science and Technology, Mianyang, 621010, China
[b] Department of Mechanical Engineering and Materials Science, Yale University, New Haven, CT, 06511, USA
[c] Department of Chemical and Environmental Engineering, Yale University, New Haven, CT, 06511, USA

ARTICLE INFO

Keywords:
Amorphous alloy
Nanoscratch
Fictive temperature
Wearless friction
Plastic deformation
Fracture

ABSTRACT

Understanding the structure-property relationship is important for guiding the design of metallic glasses with advanced properties. In this work, we employ nanoscratching experiments to establish a correlation between structure and nano-tribological behavior in Zr-based metallic glasses where the structural state of the material is characterized by its fictive temperature, T_f. The results indicate that independent of the applied load, the scratching depth and residual depth of the scratch track increase with an increase in T_f, which is ascribed to the increase in free volume that metallic glasses experience when they are prepared with higher T_f. Furthermore, it was found that the effect of T_f on the friction coefficient varied significantly with the applied load: At low loads, adhesion-induced friction dominates so that low-T_f samples display higher friction coefficients, which we correlate to their denser packed structure affecting interfacial shear. At high loads, however, plowing becomes dominant, which causes the friction coefficient of low-T_f samples to become lower than the ones of high-T_f samples and is ultimately a consequence the higher elastic recovery capability for the samples with lower T_f. Meanwhile, sudden sink-in events of scratching depth are observed when ramping the load during nano-scratching in the indenter face forward direction, revealing the occurrence of scratch-induced yielding. Thereby, the higher degree to which free volume is available in high-T_f samples causes them to show higher plasticity, which in turn is responsible for the higher critical loads at which the sink-in event occurs. This finding implies the possibility of using ramping load scratching to characterize the ductile-to-brittle transition of metallic glasses as an alternative to carrying out time-consuming fracture tests.

1. Introduction

Metallic glasses, which represent a distinct class of materials that was first introduced in 1960 [1], exhibit promising potential in many engineering applications due to their attractive mechanical properties, such as high strength, large elastic limit, and superior wear resistance [2–5]. However, unlike crystalline alloys in which the atomic structure featuring periodic translational arrangement of atoms is explicitly known, the exact structure of metallic glasses is difficult to characterize due to the complexity of the disordered atomic arrangements that metallic glasses represent [6]. The most recent developments in glass mechanics aim to correlate structural disorder and mechanical behaviors, in particular, the relations between glassy disorder and the mechanical properties of glasses – e.g., stiffness, strength and fracture toughness [7]. The relationship between the properties of metallic glass and structure, which can be tuned by setting the glass' degree of relaxation, has become the focus of metallic glass studies [8]. Nevertheless, more attempts need to be made to deepen the understanding of the relationship between the metallic glass' structure and its tribological properties, which is crucial to develop an ability to tailor metallic glass alloys for tribological applications.

To manipulate the structure of a metallic glass and, with it, many of

* Corresponding author.
** Corresponding author.
E-mail addresses: yujiaxin@swust.edu.cn (J. Yu), amit.datye@yale.edu (A. Datye).
[1] Wanfu Dong and Jianping Lai contributed equally to this work.

https://doi.org/10.1016/j.wear.2022.204247
Received 13 December 2021; Received in revised form 10 January 2022; Accepted 14 January 2022
Available online 19 January 2022

its properties, thermal treatments are applied [9,10]. However, the annealing protocols that have been typically used by researchers in the past were mostly phenomenological in nature and led frequently to non-reproducible properties in the bulk material. This issue can be circumvented by introducing the concept of a 'fictive temperature' T_f to specify the basic features of structural states [9–13]. Thereby, a metallic glass is said to attain a certain T_f when it is annealed at that temperature for long enough to obtain a 'fully relaxed' structure but short enough to not undergo any crystallization, where the time needed to achieve that state is estimated by the Vogel-Fulcher-Tammann (VFT) equation [14–16]. In particular, T_f has been confirmed to have a strong correlation with free volume. For instance, for metallic glasses treated at a higher T_f, the viscosity of supercooled liquid at the T_f is lower, leading to a less dense packing of atomic structure upon quenching and thus to a higher fraction of free volume [17–19]. Therefore, the T_f can be regarded as an adequate indicator of a well-defined structural state that features a reproducible amount of free volume and, consequently, similar short-range atomic ordering. Previous researchers [9,20–23] have used T_f to describe the structural evolution during deformation processes in terms of free volume. For example, Ketkaew [20] and Kumar [21] examined the plasticity of Zr-based, Pd-based, and Pt-based bulk metallic glasses (BMGs) that were treated at different T_f and found a corresponding mechanical transition from brittle to ductile with increasing T_f, which they explained in terms of free volume. In addition, since metallic glasses are in a metastable equilibrium when they are quenched from a certain annealing temperature, the hardness of metallic glasses is affected by the amount of free volume and changes in short-range order, which is associated with the magnitude of T_f [22]. This relationship has been further corroborated in two of our previous publications, where we found that the hardness and moduli of metallic glasses decreased with an increase in T_f and that changes in free volume and ordering were primarily responsible for the changes in mechanical properties [9,23].

Although relevant correlations between T_f and mechanical properties have been established, very few studies have focused on the effect of T_f on the nanoscale tribological properties of BMGs. It was reported that the changes in structural heterogeneity led to the fluctuation of tribological properties of Zr-BMG [24]. Since the T_f is closely correlated with the structure of BMGs in terms of free volume and short-range order [25], it is reasonable to deduce that the changes in T_f would exert a significant effect on the nanoscale friction and plastic deformation in BMGs. Further work deserves to be made to confirm this point.

Recent applications of BMGs enabled by atomic scale imprinting by using thermoplastic forming [10,26–29] to develop nanostructures for coating applications and developments in materials discovery of glasses for biomedical [30] and mechanical [31] applications etc. has shown the need to understand the nanotribological properties of the metallic glasses. In this work, we investigate the nanoscratching behavior of BMGs subjected to heat treatment at different T_f, which can control the structure of BMG, and discuss the intrinsic factors affecting the nanoscratching properties of BMGs. Furthermore, the difference in the response of friction coefficient with increasing applied load is observed for BMGs with various T_f, where the role of adhesive friction vs. plowing friction was clarified during nanoscratching. Most notably, the comparison of friction coefficient between experimental data and predicted values by the derived theoretical model demonstrates the validity of the model in assessing the friction coefficient of metallic glasses in ploughing-dominated friction regime. The tribological applications can tailored purposely by selecting those metallic glasses with desired hardness and elastic recovery capability.

2. Materials and methods

2.1. Sample preparation

The bulk metallic glass (BMG) with a composition of $Zr_{44}Ti_{11}Cu_{10}Ni_{10}Be_{25}$ (atomic fraction) was purchased from Materion (Mayfield Heights, Ohio) and is referred to as Zr-BMG throughout the paper. The as-cast Zr-BMG samples were thermoplastically formed by heating at 420 °C for 2 min under a compressive force of 1 kN followed by a subsequent water quench to eliminate most of the casting defects. The samples were then cut into small cubes and were first annealed at a certain temperature for a period time and then quenched into the water. Annealing at temperatures below the alloy's crystallization temperature T_x, which was previously identified as 466 °C [23], was then employed to set a sample's 'fictive temperature' T_f. Thereby, the holding time during annealing needed to be shorter than the time required to reach the onset of crystallization at that temperature, but long enough for full structural relaxation to occur, which can be determined using the VFT equation mentioned in the introduction [14–16]. Accordingly, the structural relaxation time was calculated to be about 6 h for a T_f of 320 °C, 32 s for a T_f of 370 °C and 0.7 s for a T_f of 410 °C, respectively. Referring to our previous DSC results [23], the time needed to reach the onset of crystallization was estimated to exceed 10 years for an annealing temperature of 320 °C, about 100 min for annealing at 370 °C, and about 12 min for annealing at 410 °C, respectively. To achieve complete structural relaxation but avoid even the slightest possibility of crystallization, the holding time at each temperature was selected to be 1.5 times the relaxation time calculated by VFT equation. The annealing temperature is then referred to as the fictive temperature T_f, and each T_f is understood to represent a well-defined structural state.

Prior to the nanoindentation/nanoscratch tests, all the Zr-BMG samples were first mechanically polished, then cleaned in ethanol with an ultrasonic cleaning machine for 5 min, rinsed with pure water, and finally dried using high-purity nitrogen. For such samples, the root-mean-square (RMS) roughness was measured by white light scanning profilometry (MFT-3000, Rtec, San Jose, CA) to be 5.5–6.4 nm in a 100 μm × 100 μm area.

2.2. Experimental methods

The mechanical properties and nano-tribological behavior of Zr-BMGs were measured by a nanoindenter/nanoscratch instrument (Keysight G200, Santa Rosa, CA, USA). During nanoindentation testing, a diamond Berkovich indenter (Micro Star Technology, Huntsville, TX, USA) with a nominal radius of ≈20 nm was used, and the area function of the indenter was calibrated using a standard fused silica sample before tests to ensure accurate experimental data. The loading rate was set to 0.2 mN/s and the holding time at peak load (3 mN) was 2 s. 16 tests were repeated for each sample to obtain reliable results. The hardness and reduce modulus were measured to be 7.98 ± 0.25 GPa and 108.35 ± 0.69 GPa, respectively, for samples with T_f = 320 °C, 7.70 ± 0.27 GPa and 105.32 ± 1.05 GPa for samples with T_f = 370 °C, and 7.45 ± 0.16 GPa and 102.41 ± 0.57 GPa for sample with T_f = 410 °C.

Both constant and ramping loading modes were carried out in the nanoscratching tests, in which a cube corner indenter from Micro Star Technology with a nominal radius of ≈50 nm was used. In constant load scratching, the scratching speed is 10 μm/s and scratching distance is 100 μm. To investigate the scratch-induced deformation at elastic- and plastic-dominated deformation conditions clearly, three normal loads were selected: 0.8 mN, 1 mN and 3 mN. The scratching direction was set as indenter edge forward, which could lead to a relatively weak plastic deformation response due to the relatively low contact stress and shallow scratch depth compared to the other scratching directions [32]. After scratching, the cross-sectional profile of the scratch track was captured by scanning the middle of the tracks using the same tip with the low load of 20 μN.

In ramping load scratch experiments, the normal load ranges from 20 μN to 3 mN, the scratching speed is 10 μm/s, and the scratching distance is 100 μm. The scratching direction was set as both indenter edge forward and face forward direction, respectively, to compare the differences in deformation behavior of the BMG when the sample is

exposed to different frictional shear stress fields. The position where the cross-profiles of the residual grooves were scanned was visualized using an optical microscope (Olympus BX-51P, Japan). The surface images of ramping load scratching tracks were examined using a scanning electron microscope (SEM, Zeiss Ultra 55, Oberkochen, Germany). For both constant and ramping load nanoscratching, the friction coefficient and scratching depth were collected in real time, and the residual depth of scratching tracks can be obtained by the indenter post-scanning process. All the constant/ramping load nanoscratching tests on each sample was repeated 8 times to ensure the accuracy of experimental results.

3. Results and discussion

3.1. Effect of fictive temperature on the tribological behaviors of Zr-BMGs in constant load nanoscratching

Fig. 1 shows the representative results of nanoscratch tests under three constant loads on Zr-BMGs with various T_f. From Fig. 1a–c, it is evident that the scratching depth at peak load increases with the increase in T_f, independent of the normal load. The scratching depth h increases from ≈22 nm to ≈30 nm for the lower-load condition of 0.8 mN, from ≈40 nm to ≈70 nm for the intermediate-load condition of 1 mN, and from ≈130 nm to ≈220 nm for the higher-load condition of 3 mN when T_f increases from 320 °C to 410 °C. These findings are in full agreement with the expectation that BMGs with higher T_f have more free volume and thus looser atomic packing, which results in both a weaker resistance to scratch-induced deformation as well as greater plasticity. After scratching, some recovery can be observed (dashed lines in Fig. 1a–c); here, the residual depths h_r of the scratching tracks become ≲1 nm, ≈1 nm, and ≈2 nm for the scratches performed with a load of 0.8 mN, ≈4 nm, ≈7 nm, and ≈9 nm for the scratches performed with a load of 1 mN, and ≈60 nm, ≈100 nm, and ≈150 nm for the 3 mN scratches, where the three values represent in each case the findings obtained on the Zr-BMG samples prepared with T_f's of 320 °C, 370 °C, and 410 °C, respectively. These results can now be used to calculate the elastic recovery index η [33,34], which is defined as the ratio of recovery depth to the scratching depth $\eta = (h\text{-}h_r)/h$ and can be used to assess the elastic recovery capacity of metallic glass in the scratching test after unloading as a function of its fictive temperature. As shown in Table 1, when T_f increases from 320 °C to 410 °C, the elastic recovery index decreases from 0.96 to 0.93 for the load of 0.8 mN, from 0.91 to 0.88 for the load of 1 mN, and from 0.57 to 0.31 for the load of 3 mN.

Fig. 1d–f show representative cross-sectional profile lines obtained in the middle of the nanoscratch track for each load. It was found that the scratch-induced pile-up and groove was far more obvious for the sample with a higher T_f in 3 mN load conditions. The estimated volumes of pile-up $V_{pile\text{-}up}$, groove V_{groove}, and total plastic deformation V ($V = V_{pile\text{-}up} + V_{groove}$) are quantified in Table 1 for all constant load experimental runs carried out with 1 mN and 3 mN loads, while no clear quantification was possible for runs with 0.8 mN load. Both of $V_{pile\text{-}up}$ and V_{groove} are found

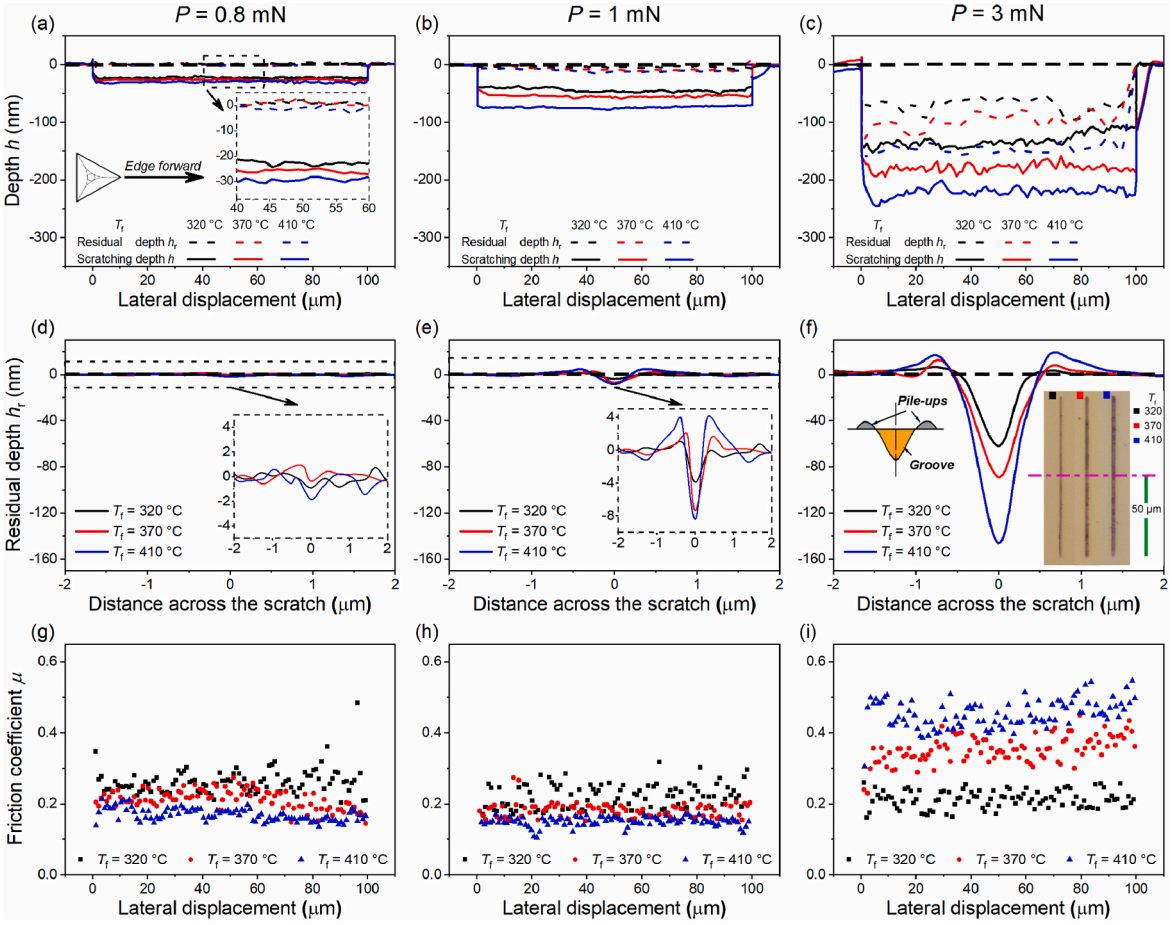

Fig. 1. The representative results of nanoscratching tests under three different constant loads in Zr-BMGs prepared with three distinct T_f, where the indenter scratches in edge forward direction. (a, b, c) The scratching depth and residual depth profiles under a constant load of 0.8 mN (a), 1 mN (b), and 3 mN (c), where the inset in (a) denotes the scratching direction of the indenter. (d, e, f) Cross-sectional profile lines obtained in the middle of the nanoscratch tracks for the 0.8 mN scratch (d), 1.0 mN scratch (e) and the 3 mN scratch (f). The inserted image in (f) indicates the position (the pink line) where the cross-profiles of the residual grooves are scanned. Finally, (g), (h), and (i) display the friction coefficients measured during scratching for the three loads. (For interpretation of the references to colour in this figure legend, the reader is referred to the Web version of this article.)

Table 1
Summary of the calculated elastic recovery index (η), pile-up volume ($V_{\text{pile-up}}$), groove volume (V_{groove}), and the deformation volume (V) of scratching tracks in Zr-BMGs prepared with various T_f, as extracted from Fig. 1. Since the 0.8 mN case is virtually fully elastic, no definite values is put into the table to quantify the deformation volume.

Load (mN)	T_f (°C)	η	$V_{\text{pile-up}}$ ($\times 10^{-3}\mu m^3$)	V_{groove} ($\times 10^{-3}\mu m^3$)	V ($V_{\text{pile-up}}$ + V_{groove}) ($\times 10^{-3}\mu m^3$)
0.8	320	0.96 ± 0.04	/	/	/
	370	0.96 ± 0.06	/	/	/
	410	0.93 ± 0.04	/	/	/
1	320	0.91 ± 0.02	0.81 ± 0.09	2.37 ± 0.12	3.18 ± 0.21
	370	0.89 ± 0.03	1.31 ± 0.11	3.20 ± 0.26	4.51 ± 0.38
	410	0.88 ± 0.03	2.85 ± 0.53	4.00 ± 0.67	6.85 ± 1.21
3	320	0.57 ± 0.07	9.66 ± 2.04	23.89 ± 4.77	33.55 ± 6.81
	370	0.42 ± 0.05	11.72 ± 2.11	49.32 ± 5.62	61.04 ± 7.73
	410	0.31 ± 0.06	15.45 ± 3.15	75.11 ± 8.19	90.56 ± 11.94

to be larger for samples with a higher T_f. This is in line with expectations as the pile-up volume is closely related to the plastic deformation ability of metallic glasses [35–38], which is greater in sample with higher T_f as they feature more free volume than lower-T_f samples. The structure of higher-T_f samples therefore offers in comparison more potential sites for shear band formation [39], which facilitates plastic deformation under frictional shear stress [18,40] and ultimately leads to more pile-up during scratching. Furthermore, the lower hardness of the sample with a higher T_f contributes to the worse wear resistance [41,42], resulting in a deeper groove and larger deformation volume.

In addition to the scratching depth, we also investigated how the friction coefficient varies with the material's T_f for the three different normal loads employed. With the 0.8 mN load (Fig. 1g), the friction coefficient decreases from 0.24 ± 0.04 to 0.18 ± 0.02 when T_f increases from 320 °C to 410 °C, which is identical with the trend in the intermediate-load condition of 1 mN, but is opposite of what it does during the higher-load condition of 3 mN (Fig. 1i), where the friction coefficient increases from 0.21 ± 0.03 to 0.46 ± 0.04. Nevertheless, the nanoscale friction behavior depends in both cases on T_f and load.

To understand this seemingly contradictory behavior, let us recall Bowden and Tabor's theory of metallic friction [43]. To explain the mechanisms that occur when moving a hard slider over a metal surface, they started by recognizing that even highly polished surfaces like we have them in the current experiment are still "rough" at the nanometer scale. This means in effect that only a fraction of the "apparent" contact area A_{app} is actually touching, which reduces the slider-substrate contact to the sum of a large number of single asperities; a heuristic approach that due to the complexity of realistic interfaces took decades to be put on solid theoretical footing first by Greenwood and Williamson [44] and then, with a greatly improved approach, by Persson and Tosatti [45,46]. Bowden and Tabor then suggested to split the frictional force F as the sum of two contributions called F_S and F_P. They rationalized this approximation arguing that asperities basically have two options: If they are producing "deep" scratches while moving, most work needed to drag the slider forward is likely to go into the action of pushing atoms out of its way, which is reflected in the "plowing" term F_P. In contrast, F_S denotes the force needed to shear asperities that don't produce much visible scratching (as it is for the 0.8 mN load in our work). In that case, adhesion will dominate any effort to shear metallic asperities, as most work to sustain the slider's motion then goes into "ripping" single-asperity contacts apart that continuously form.

Inspired by this model, we are splitting the measured friction coefficient μ into two contributions, with one describing adhesive friction through a friction coefficient μ_a and one arising from plowing friction with an associated friction coefficient μ_p. For the 0.8 mN case, the elastic recovery index of the scratching track is around 0.93 ~ 0.96, which implies that despite some scratching adhesive friction should be substantial. For that case, Bowden and Tabor proposed that friction, and with it the adhesive friction coefficient μ_a, will be proportional to the total value of the adhesive force F_{ad} that needs to be overcome, which is proportional to the "real" area the slider touches during sliding A_{real}. Since the estimated indenter radius ($R \approx 50$ nm) is almost equal to the scratching depth, the Hertzian sphere-plane contact model can be used for analysis, resulting in Refs. [41,42,47]:

$$\mu_a = \pi\left(\frac{3R}{4}\right)^{2/3} \cdot P^{-1/3} \cdot \frac{\tau_s}{(E_r)^{2/3}} \quad (1)$$

Here, P reflects the normal load, τ_s the interfacial shear strength, and E_r the reduced modulus; also note that because the Hertz model recovers the "apparent" contact area A_{app} and not the actual one, τ_s will also represent an "apparent" interfacial shear strength that depends on the details of interface roughness rather than an accurate, material-specific value for atomically well-defined surfaces sliding. However, since $A_{app} \propto A_{real}$, $\tau_s \propto \tau_{s\text{-}real}$ with the same proportionality factor. Nevertheless, this equation ultimately indicates that for a fixed indenter and at a constant normal load, μ_a is only related to $\tau_s/(E_r)^{2/3}$. Using the measured friction coefficient values from Fig. 1 and the reduced moduli for each sample found in the previous section and neglecting any potential contribution from plowing, τ_s can be calculated as 14.35 ± 2.16 GPa, 13.24 ± 1.53 GPa, and 11.67 ± 1.37 GPa for the Zr-BMG samples with T_f = 320 °C, 370 °C, and 410 °C, respectively.

This decrease of interfacial shear strength with increasing T_f can be correlated with the different structure among Zr-BMGs. In general, adhesion, and thus the interfacial shear strength during adhesive friction, are mainly determined by electrostatic, capillary, and van der Waals forces as well as the chemical bonding between slider and sample [48–53]. Since no net charges are expected to remain on indenter and sample surfaces, the electrostatic forces can be neglected. Due to identical experimental humidity and temperature environment and the similar surface energy for all the Zr-BMGs (the water contact angle of three samples was measured as 83 ~ 85°, thus, there is no significant difference), the effect of differences in the capillary force is similarly improbable to cause much of the observed variations. The van der Waals force and, most importantly, the chemical bonding forces between metal atoms at and near the interface can then be regarded as the variables affecting interfacial shear strength between Zr-BMGs with various T_f and indenter. When the diamond indenter scratches the sample, the possibility the van der Waals [50,54] and chemical forces [51,53] per unit area at the slider-sample interface are higher for the Zr-BMGs with a denser atomic structure, which may contribute to the increased interfacial shear strength. While this is likely a relatively small effect, we have seen above that most work to sustain the slider's motion then goes into ripping single-asperity contacts apart that continuously form. Since the low-T_f samples are denser, they are more difficult to deform (both elastic and plastic) and more mechanical work needs to be done to rupture the contacted asperities between the indenter and sample, which may then explain the higher friction coefficient for the samples with lower T_f.

When the normal load is 3 mN, the scratching depth is much deeper than the estimated indenter radius of approx. 50 nm, thus the sphere-plane contact model [41,42] becomes invalid, and triangular pyramid-plane contact model [55] needs to be considered. Fig. 2 schematically shows the sliding contact model between a perfectly cube corner indenter and plane sample, where the indenter is scratching in edge-forward direction. In this orientation, the contribution of elastic

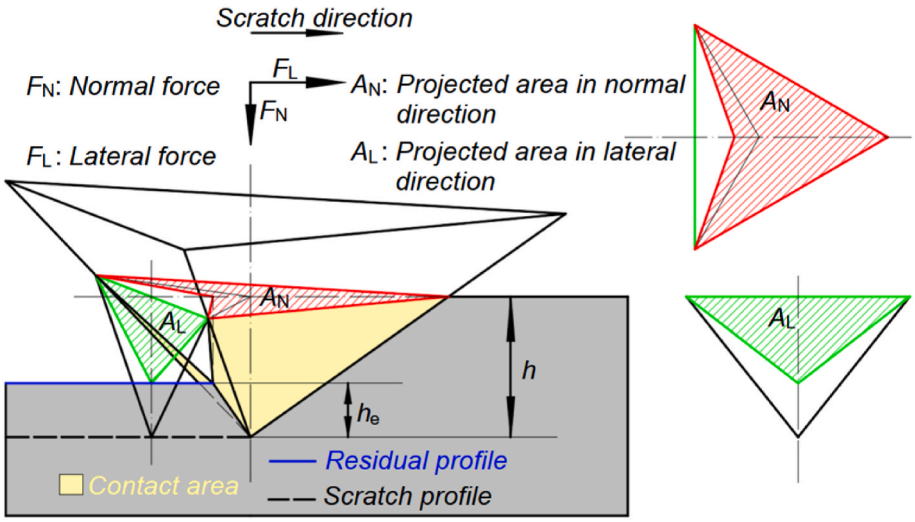

Fig. 2. Schematic illustration of contact between cube corner indenter and plane sample during nanoscratching with indenter edge forward direction. The projected areas in normal (red), A_N, and lateral (green) directions, A_L, are schematically shown, in which the contribution of elastic recovery to the projected areas has been taken account. (For interpretation of the references to colour in this figure legend, the reader is referred to the Web version of this article.)

recovery to the projected areas has been taken account. At a peak load of 3 mN, the elastic recovery index is in the range of 0.31 ~ 0.57 for all samples, indicating significant plastic deformation and thus the plowing friction plays a more important role. The plowing friction coefficient μ_p is defined as $\mu_p = A_L/A_N$ [56–58], where A_L and A_N are the projections of the contact area in the lateral and normal directions, respectively, as illustrated in Fig. 2. Considering the contact geometry between cube corner indenter and plane sample, A_L and A_N can be written as Eqs. (2) and (3):

$$A_L = \frac{\sqrt{6}}{2} h \cdot (h - h_e) \tag{2}$$

$$A_N = \sqrt{3} h^2 + \frac{\sqrt{3}}{2} h \cdot h_e \tag{3}$$

where h, h_e, and h_r are the scratching depth, elastic recovery depth, and residual depth, respectively, and h, h_r can be directly captured from Fig. 1c. Therefore, the plowing friction coefficient μ_p can be rewritten as:

$$\mu_p = \frac{A_L}{A_N} = \frac{\sqrt{2}(h - h_e)}{2h + h_e} \tag{4}$$

Substituting the elastic recovery index $\eta = h_e/h$, Eq. (4) can be rewritten as Eq. (5)

$$\mu_p = \frac{\sqrt{2}(1 - \eta)}{2 + \eta} \tag{5}$$

which reveals that the plowing friction coefficient is only related to η.

Fig. 3 shows the measured friction coefficient as a function of elastic recovery index for the three Zr-BMGs with various T_f. By comparison, the measured friction coefficient provided a good fit with the theoretical plowing friction coefficient for the three samples, which further reveals that the plastic deformation induced plowing friction dominates the friction mechanism for nanoscratches at 3 mN constant load. For the metallic glasses with a low T_f, the structural packing is denser than its counterpart with a high T_f, so the spacing between adjacent atoms should be smaller, giving rise to a larger cohesive force. Benefited from the denser packing structure, the metallic glasses with a lower T_f feature a higher elastic modulus, hardness, and stronger recovery capability. The stronger recovery capability with decreasing T_f contributes directly to the lower friction coefficient, as calculated by Eq. (5).

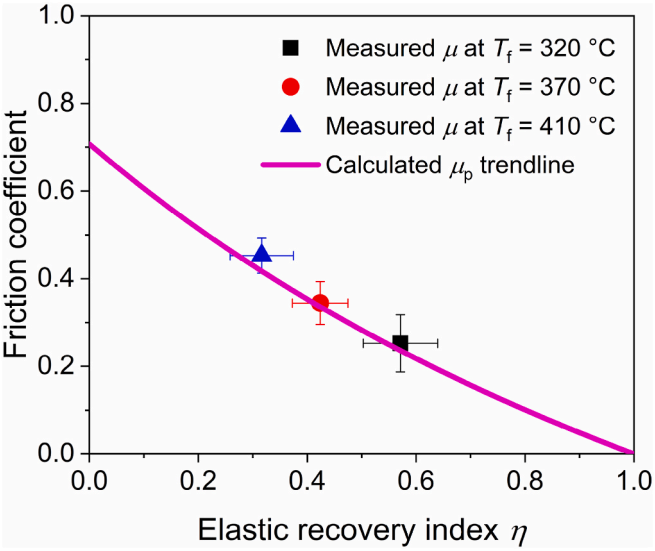

Fig. 3. The measured friction coefficient on Zr-BMGs with various T_f as a function of elastic recovery index η under the normal load of 3 mN, where the pink line presents the plowing friction coefficient calculated from Eq. (5). (For interpretation of the references to colour in this figure legend, the reader is referred to the Web version of this article.)

3.2. *Effect of fictive temperature on the tribological behaviors of Zr-BMGs under ramping load nanoscratching*

Fig. 4 shows the representative scratch/residual depth and friction coefficient versus load/lateral displacement during a ramping load scratching experiment from 0 to 3 mN, where the scratches are made in the indenter edge forward direction. Here, scratching in an entirely elastic deformation regime is labeled as region I, which is evidenced by the full recovery of surface from the residual depth profiles. Correspondingly, the regime where plastic deformation occurs is labeled as region II. Fig. 4a indicates that both the scratching and residual depth are deeper with a higher T_f in region II, which is consistent with the results found in the constant load nanoscratching tests.

In region I, the friction coefficient decreases sharply as the applied load increases until ≈0.55 mN, as shown in Fig. 4b, thereby replicating

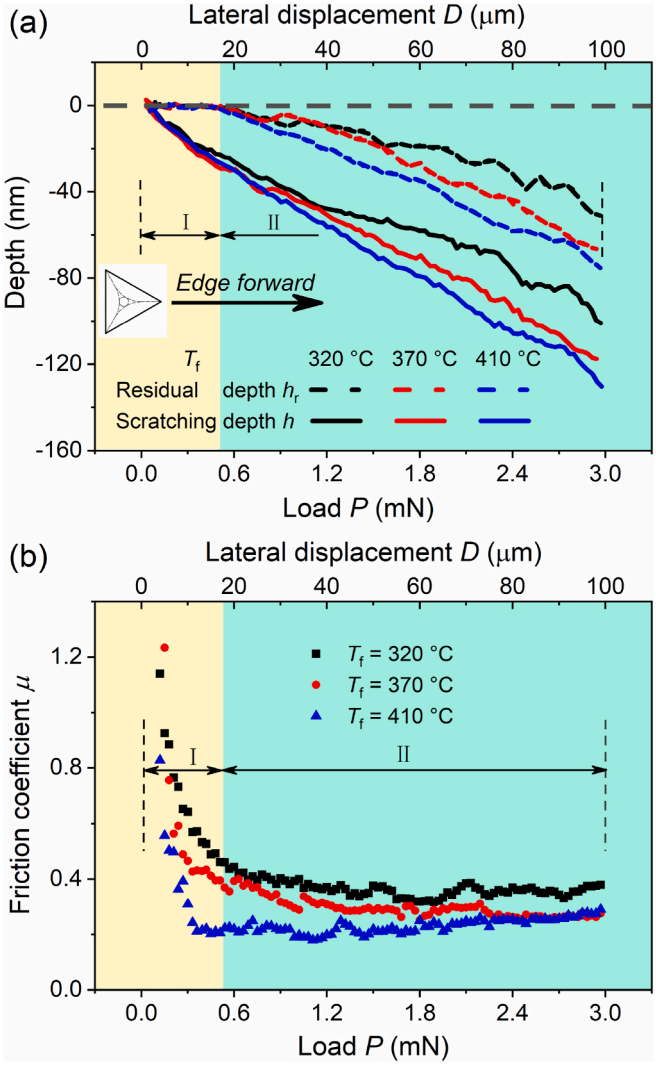

Fig. 4. (a) The representative scratching depth and residual depth profiles of the Zr-BMGs with various T_f under a ramping load scratching, where the scratching direction is indenter edge forward direction; (b) friction coefficient during ramping load scratching in the Zr-BMGs with various T_f. Region I is defined as scratching in an entirely elastic deformation regime and region II is defined as scratching in a regime where plastic deformation occurs.

trends that were found in earlier publications for adhesion-controlled friction [41,42]. Although featuring similar decreasing behaviors, the friction coefficient is highest for the Zr-BMGs with T_f of 320 °C, followed by the sample with 370 °C and 410 °C, respectively, which agrees well with the findings of Fig. 1g and their related discussion.

When the applied load exceeds 0.6 mN (region II), plastic deformation starts to occur, and the effect of plowing becomes more prominent. Note, however, that the scratching depth under constant load scratching (≈130 nm, ≈180 nm, and ≈220 nm, respectively, for the three samples from Fig. 1c) at 3 mN load is higher when compared to the scratching depth at 3 mN peak load in ramping load experiments (≈100 nm, ≈110 nm, and ≈130 nm for the three samples). A possible explanation for this discrepancy could be that for the same scratching depth, the contact area between indenter and sample is larger for ramping load than constant load scratching, as there are fewer atoms at the indenter's back side that have already been removed. To then achieve the same contact area under both conditions, the scratching depth has to be lower for ramped-load experiments than for constant-load experiments. Similar experimental phenomena were also observed in some other nanoscratch works [59,60].

Under such a scenario, the scratching depth at maximum load may then still be insufficient to induce a fully plowing-dominated friction mechanism in region II as it did in for constant-load scratching. As a result, the friction coefficient is still highest for the Zr-BMG with a T_f of 320 °C while the ones for the Zr-BMGs with T_f of 370 °C and 410 °C, respectively, are almost equal when the applied load exceeds 2.4 mN (Fig. 4b), which is reversed from the results of the constant load scratching at 3 mN (see Fig. 1i). It is, however, to be expected that with further increasing load, and thus increasing scratching depth, plowing friction will ultimately dominate and the trend lines for the friction coefficient with load should cross over to align with the findings of constant-load scratching.

In addition to the indenter edge forward direction scratching shown so far, we also carried out experiments with ramping load in the indenter face forward direction, which creates deeper scratching depth without changing the peak load condition [32,61]. Fig. 5a shows representative scratch and residual depth profiles in the three Zr-BMGs. Similar to the results in edge forward direction, both the scratching and residual depth are deeper in sample with higher T_f. However, the maximum scratching depth with indenter face forward direction is much deeper, ranging from ≈210 nm to ≈300 nm at the maximum load of 3 mN. Another distinct feature is that when with the normal load approaches approx. 1.8–2.4 mN, a sink-in event can be observed in the scratching depth, accompanied by a corresponding jump in friction coefficient for all samples. As seen in Fig. 5b, the critical load P_c at which the sink-in event occurs is higher for samples with higher T_f.

The sink-in event is believed to be associated with the scratch-induced yielding of metallic glasses under frictional shear stress, which means onset of ductile fracture [62]. The load drop or displacement burst in nanomechanics, similar to the sink-in event, was closely related to the shear banding event, which was essentially the deformation carrier of metallic glasses in inhomogeneous deformation regime [63]. Since we have already seen above that the free volume retained in the structure of BMGs, and thus their plasticity, increases with increasing T_f [23], more possible spatial sites for shear bands nucleation are available in BMGs with higher T_f, which facilitates the formation of shear bands [39,64–66]. The resulting enhanced ability to alleviate external pressure by plastic deformation effectively suppresses scratch-induced yielding, making the sample with a higher T_f to ductile fracture [67–69] at a higher normal load. The results in Fig. 5b also agree well with the research by Ketkaew [20] and Kumar [21], who demonstrated using fracture tests that the fracture toughness of Zr-BMGs increased with an increasing T_f, especially, especially when T_f was higher than the glass transition temperature T_g. As a result, ramping load nanoscratch tests with indenter face forward direction may provide an easier avenue to characterize the brittle-to-ductile transitions in metallic glass compared with traditional fracture tests, which are very time-consuming to carry out.

Next, we observe that the relative behavior of the measured friction coefficient μ with load P for the three Zr-BMGs in indenter face forward scratching, shown in Fig. 5c, is different from indenter edge forward scratching. For a "low" load condition, i.e., with loads that are lower than 0.3 mN, the friction coefficient is highest for the sample with T_f = 320 °C, following by the samples with T_f = 370 °C and 410 °C. This is reversed in a "high" load condition with loads larger than 2.4 mN, where the friction coefficient is highest for the sample with T_f = 410 °C, following by the samples with T_f = 370 °C and 320 °C. The results are in good agreement with the constant loading scratching results, as shown in Fig. 1, and our related discussion, which assigned the reversal of the friction coefficient sequence with increasing loads to the different friction mechanisms dominating under the various applied conditions.

For further analysis, we note that in indenter face forward scratch experiments, the geometric formula of projected area in normal direction A_N becomes $A_N = \sqrt{3}h^2/2 + \sqrt{3}h \cdot h_e$, so the plowing friction coefficient μ_p can be calculated as Eq. (6):

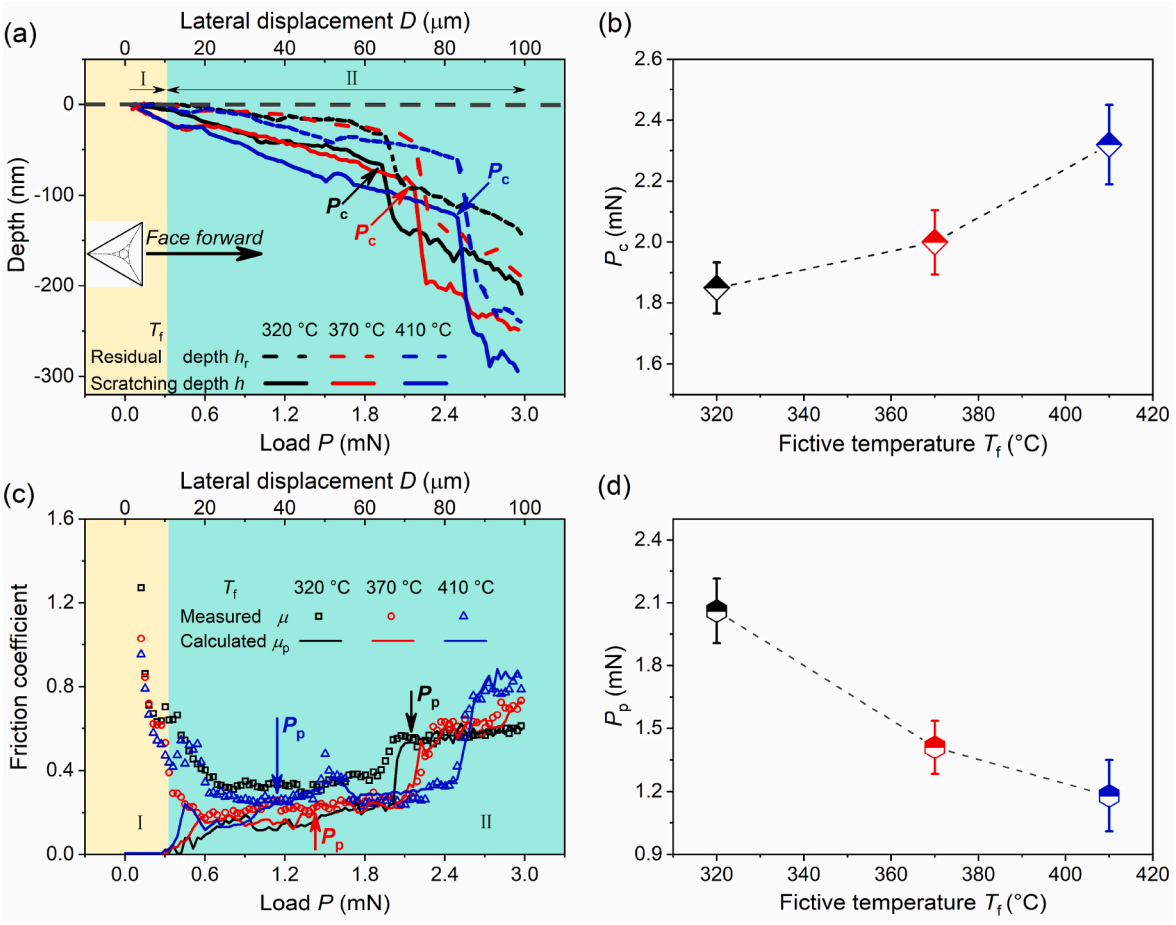

Fig. 5. (a) The representative scratching depth and residual depth profiles in the Zr-BMGs with various T_f in a ramping load scratching, where the scratching direction is indenter face forward direction. During the ramping, the critical load experiences sink-in events that are marked with P_c. (b) The critical load values P_c at which a sink-in event occurs plotted as a function of the fictive temperature T_f. (c) The plowing friction coefficient as calculated via Eq. (6) (solid lines) and the measured friction coefficient of the various Zr-BMGs (discrete points) as a function of the load where the arrows show the intersecting load P_p between calculated and measured friction coefficient. (d) P_p as a function of T_f. The region I is defined as complete elastic deformation region and regime II is defined as plastic deformation occurring region. Note that the error bars in (b) and (d) are calculated by averaging P_c and P_p from at least six curves rather than from a single curve.

$$\mu_p = \frac{A_L}{A_N} = \frac{\sqrt{6}h\cdot(h-h_e)/2}{\sqrt{3}h^2/2 + \sqrt{3}h\cdot h_e} = \frac{\sqrt{2}(1-\eta)}{1+2\eta} \tag{6}$$

Using the scratching depth and residual depth as extracted from the data in Fig. 5a, the elastic recovery index η can be recovered, from which the theoretical plowing friction coefficient μ_p was calculated and plotted as solid lines in Fig. 5c. It was found that the calculated μ_p increases with increasing applied load and intersects with measured friction coefficient at a certain load P_p, highlighted by arrows in Fig. 5c, suggesting that plowing-dominated friction is established when the load attains P_p. Fig. 5d then reveals that with an increase in T_f, P_p decreases, which simply means that in line with our above observations and discussions, plowing occurs more easily at the same load condition.

Finally, Fig. 6 shows scanning electron microscopy (SEM) images of three scratching tracks for Zr-BMGs with various T_f for the ramping load scratching in edge forward and face forward directions, respectively. For both scratching directions, the length of elastic deformation stage is longer for the sample with a lower T_f, as indicated by the absence of scratching marks, suggesting the similar effect of T_f on the resistance to elastic deformation of metallic glasses. A close observation reveals that for both scratching directions, the scratching grooves created by the diamond indenter get wider and deeper as the T_f increases from 320 °C to 410 °C. The increase of hardness with decreasing T_f is responsible for the changes in width and depth of scratching grooves.

Another interesting feature that should be noted is that the deformation mechanism is slightly different for the three Zr-BMGs. For the sample with T_f of 370 °C in face forward scratching case, discrete chips were observed along the edges of grooves, while continuous pile-ups and ridges were discerned along the sides of grooves without any cracking or fracture for the sample with T_f of 410 °C. This is in line with our above findings where compared to the sample with T_f of 370 °C, the free volume in the structure of the sample with T_f of 410 °C is larger, which facilitates the formation of shear bands and thereby gives rise to a higher plasticity [39,65,66]. As a result, the scratch-induced deformation occurs by ductile plowing for the sample with $T_f = 410$ °C while in the sample with $T_f = 370$ °C, the anticipated low plasticity leads to the domination of brittle behavior [20,21], as indicated by the chipping features with little ridges and pile-up along the grooves. Comparison between edge forward and face forward configurations reveals that the degree of deformation due to scratching is greater in face forward direction. For instance, the length of elastic deformation stage is shorter for each sample in face forward scratching case. In plastic deformation-dominated regime, it is obvious that the grooves for each sample in face forward scratching case are deeper and wider in comparison to its counterparts in edge forward case. All of microscopic features are consistent with the results of scratching profiles in Figs. 4 and 5.

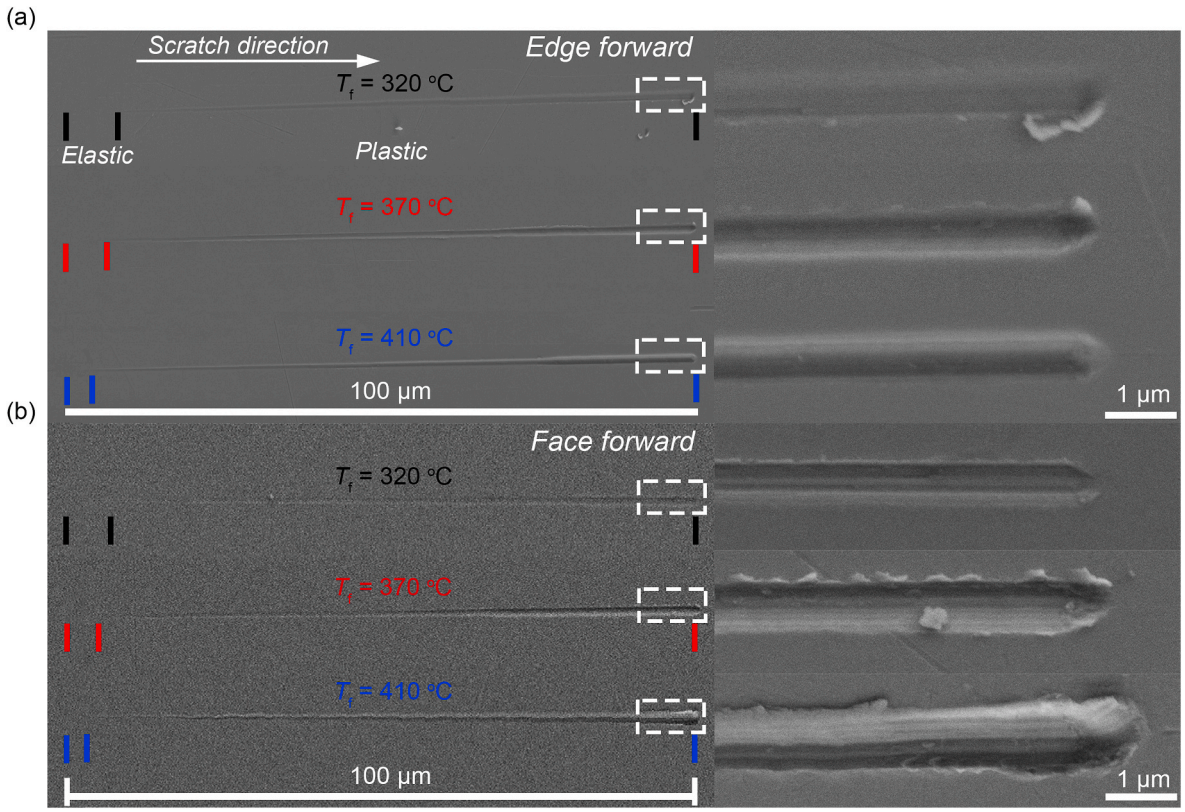

Fig. 6. Representative SEM images of scratching tracks and corresponding enlarged images of the white boxes in Zr-BMGs with various T_f for the ramping load scratching in (a) edge forward and (b) face forward direction, respectively.

4. Conclusions

In this work, nanoscratching experiments are performed on Zr-BMGs with various fictive temperatures T_f with both constant and ramping load experimental protocols to investigate the effect of T_f on the friction and deformation behavior of Zr-BMGs. The main conclusions from these experiments are summarized below.

(1) With the increase in T_f, independent of the normal load, the scratching and residual depths increase and the scratch-resistance decreases, which is ascribed to a decrease in hardness and elastic modulus of the metallic glasses.
(2) The effect of T_f on the friction coefficient of Zr-BMGs depends on the applied normal load. At low loads, adhesive friction dominates, where the Zr-BMG with a lower T_f causes a higher interfacial shear strength between sample and indenter, resulting in a higher friction coefficient. At high loads, plowing friction dominates, where the Zr-BMG with lower T_f causes higher elastic recovery index in nanoscratching, causing a lower friction coefficient.
(3) A sink-in event in scratching depth can be found in the ramping load nanoscratching in the indenter face forward direction, revealing the occurrence of scratch-induced yielding. The difference in the critical load at which the sink-in event occurs for samples with different T_f was associated with the plastic deformation ability of respective metallic glasses. As a result, the higher plasticity for the BMG with a higher T_f causes not only larger critical loads, but also more homogeneous plastic flow and continuous pile-ups, which can be observed along the scratch edge for samples with a high T_f.

Author statement

Wanfu Dong: Conceptualization, Investigation, Visualisation, Formal analysis, Methodology and Writing - Original Draft; Jianping Lai: Conceptualization, Formal analysis, Writing - review &editing and Funding acquisition; Jiaxin Yu: Conceptualization, Writing - review &editing and Funding acquisition; Udo D. Schwarz: Resources, Formal analysis, Conceptualization and Writing - review & editing; Yifan Zhang: Investigation; Kun Zhu: Investigation; Amit Datye:Formal analysis, Writing - review &editing and Funding acquisition.

Declaration of competing interest

The authors declare that they have no known competing financial interests or personal relationships that could have appeared to influence the work reported in this paper.

Acknowledgements

This work was financially supported by the National Natural Science Foundation of China (No. 51975492) and the Natural Science Foundation of Southwest University of Science and Technology (No. 19xz7163). Work by A. Datye and U. D. Schwarz was supported by the National Science Foundation of the United States (No. NSF CMMI-1901959).

References

[1] W. Klement, R.H. Willens, P.O.L. Duwez, Non-crystalline structure in solidified gold–silicon alloys, Nature 187 (1960) 869–870.
[2] W.H. Wang, The elastic properties, elastic models and elastic perspectives of metallic glasses, Prog. Mater. Sci. 57 (2012) 487–656.
[3] L. Tian, Y.Q. Cheng, Z.W. Shan, J. Li, C.C. Wang, X.D. Han, J. Sun, E. Ma, Approaching the ideal elastic limit of metallic glasses, Nat. Commun. 3 (2012) 609.
[4] H. Guo, P.F. Yan, Y.B. Wang, J. Tan, Z.F. Zhang, M.L. Sui, E. Ma, Tensile ductility and necking of metallic glass, Nat. Mater. 6 (2007) 735–739.

[5] Z.D. Sha, C.M. She, G.K. Xu, Q.X. Pei, Z.S. Liu, T.J. Wang, H.J. Gao, Metallic glass-based chiral nanolattice: light weight, auxeticity, and superior mechanical properties, Mater, Today 20 (2017) 569–576.
[6] K.J. Laws, D.B. Miracle, M. Ferry, A predictive structural model for bulk metallic glasses, Nat. Commun. 6 (2015) 8123.
[7] L. Wondraczek, E. Bouchbinder, A. Ehrlicher, J.C. Mauro, R. Sajzew, M. M. Smedskjaer, Advancing the mechanical performance of glasses: perspectives and challenges, Adv. Mater. (2021) 2109029.
[8] T.C. Hufnagel, C.A. Schuh, M.L. Falk, Deformation of metallic glasses: recent developments in theory, simulations, and experiments, Acta Mater. 109 (2016) 375–393.
[9] Z. Chen, A. Datye, P.A. Brooks, M. Sprole, J. Ketkaew, S. Sohn, J. Schroers, U. D. Schwarz, Dependence of modulus and hardness on the annealing conditions of Pt57.5Cu14.7Ni5.3P22.5 bulk metallic glass, MRS. Adv. 4 (2019) 73–79.
[10] Z. Chen, A. Datye, J. Ketkaew, S. Sohn, C. Zhou, O.E. Dagdeviren, J. Schroers, U. D. Schwarz, Relaxation and crystallization studied by observing the surface morphology evolution of atomically flat Pt57.5Cu14.7Ni5.3P22.5 upon annealing, Scripta Mater. 182 (2020) 32–37.
[11] A.Q. Tool, Relation between inelastic deformability and thermal expansion of glass in its annealing range, J. Am. Ceram. Soc. 29 (1946) 240–253.
[12] H. Kakiuchida, K. Saito, A.J. Ikushima, Fictive-temperature dependence of structural relaxation in silica glass, J. Appl. Phys. 94 (2003) 1705–1708.
[13] J.C. Mauro, R.J. Loucks, P.K. Gupta, Fictive temperature and the glassy state, J. Am. Ceram. Soc. 92 (2009) 75–86.
[14] H. Vogel, The temperature dependence law of the viscosity of fluids, Phys. Z. 22 (1921) 645–646.
[15] C.T. Moynihan, A.J. Easteal, M.A. Debolt, Dependence of the fictive temperature of glass on cooling rate, J. Am. Ceram. Soc. 59 (1976) 12–16.
[16] T. Waniuk, J. Schroers, W.L. Johnson, Timescales of crystallization and viscous flow of the bulk glass-forming Zr-Ti-Ni-Cu-Be alloys, Phys. Rev. B 67 (2003) 184203–184209.
[17] A.V.D. Beukel, J. Sietsma, The glass transition as a free volume related kinetic phenomenon, Acta Metall. Mater. 38 (1990) 383–389.
[18] W.J. Wright, T.C. Hufnagel, W.D. Nix, Free volume coalescence and void formation in shear bands in metallic glass, J. Appl. Phys. 93 (2003) 1432–1437.
[19] Z. Evenson, R. Busch, Enthalpy recovery and free volume relaxation in a Zr44Ti11Ni10Cu10Be25 bulk metallic glass, J. Alloy. Compd 509 (2011) 38–41.
[20] J. Ketkaew, W. Chen, H. Wang, A. Datye, M. Fan, G. Pereira, U.D. Schwarz, Z. Liu, R. Yamada, W. Dmowski, M.D. Shattuck, C.S. O'Hern, T. Egami, E. Bouchbinder, J. Schroers, Mechanical glass transition revealed by the fracture toughness of metallic glasses, Nat. Commun. 9 (2018) 3271.
[21] G. Kumar, P. Neibecker, Y.H. Liu, J. Schroers, Critical fictive temperature for plasticity in metallic glasses, Nat. Commun. 4 (2013) 1536.
[22] Y.T. Wang, P.F. Li, L.M. Wang, Strong dependence of the hardness on fictive temperatures in far-from-equilibrium La57.5Ni12.5Al17.5Cu12.5 metallic glasses, Intermetallics 93 (2018) 197–200.
[23] A. Datye, J. Ketkaew, J. Schroers, U.D. Schwarz, Effect of the fictive temperature on the modulus, hardness, yield strength, dynamic mechanical and creep response of Zr44Ti11Cu10Ni10Be25 metallic glasses, J. Alloys Compd. 819 (2020) 152979.
[24] S. Sawamura, L. Wondraczek, Scratch hardness of glass, Phys. Rev. Mater. 2 (2018), 092601.
[25] K.W. Park, J.I. Jang, M. Wakeda, Y. Shibutani, J.C. Lee, Atomic packing density and its influence on the properties of Cu–Zr amorphous alloys, Scripta Mater. 57 (2007) 805–808.
[26] Z. Chen, A. Datye, G.H. Simon, C. Zhou, S.A. Kube, N. Liu, J. Liu, J. Schroers, U. D. Schwarz, Atomic-scale imprinting by sputter deposition of amorphous metallic films, ACS Appl. Mater. Interfaces 12 (2020) 52908–52914.
[27] C. Zhou, A. Datye, Z. Chen, G.H. Simon, X.Z. Wang, J. Schroers, U.D. Schwarz, Atomic imprinting in the absence of an intrinsic length scale, Apl. Mater. 8 (2020) 111104.
[28] R. Li, Z. Chen, A. Datye, G.H. Simon, J. Ketkaew, E. Kinser, Z. Liu, C. Zhou, O. E. Dagdeviren, S. Sohn, J.P. Singer, C.O. Osuji, J. Schroers, U.D. Schwarz, Atomic imprinting into metallic glasses, Commun. Phys. 1 (2018) 75.
[29] J.X. Yu, A. Datye, Z. Chen, C. Zhou, O.E. Dagdeviren, J. Schroers, U.D. Schwarz, Atomic-scale homogeneous plastic flow beyond near-theoretical yield stress in a metallic glass, Comun. Mater. 2 (2021) 22.
[30] A. Datye, S. Alexander Kube, D. Verma, J. Schroers, U.D. Schwarz, Accelerated discovery and mechanical property characterization of bioresorbable amorphous alloys in the Mg-Zn-Ca and the Fe-Mg-Zn systems using high-throughput methods, J. Mater. Chem. B. 7 (2019) 5392–5400.
[31] J.P. Lai, W. Hu, A. Datye, J.B. Liu, J. Schroers, U.D. Schwarz, J.X. Yu, Revealing the relationships between alloy structure, composition and plastic deformation in a ternary alloy system by a combinatorial approach, J. Mater. Sci. Technol. 84 (2021) 97–104.
[32] Y.D. Yan, T. Sun, Y.C. Liang, S. Dong, Effects of scratching directions on AFM-based abrasive abrasion process, Tribol. Int. 42 (2009) 66–70.
[33] N. Xu, W.Z. Han, Y.C. Wang, J. Li, Z.W. Shan, Nanoscratching of copper surface by CeO2, Acta Mater. 124 (2017) 343–350.
[34] S. Sanyal, S. Chabri, S. Chatterjee, N. Bhowmik, A.K. Metya, A. Sinha, Tribological behavior of thermomechanically treated Al–Mg–Si alloy by nanoscratch measurements, Tribol. Int. 102 (2016) 125–132.
[35] W.H. Wang, Dynamic relaxations and relaxation-property relationships in metallic glasses, Prog. Mater. Sci. 106 (2019) 100561.
[36] D. Lahiri, J. Karp, A.K. Keshri, C. Zhang, G.S. Dulikravich, L.J. Kecskes, A. Agarwal, Scratch induced deformation behavior of hafnium based bulk metallic glass at multiple load scales, J. Non-Cryst. Solids 410 (2015) 118–126.
[37] L. Cheng, Z.M. Jiao, S.G. Ma, J.W. Qiao, Z.H. Wang, Serrated flow behaviors of a Zr-based bulk metallic glass by nanoindentation, J. Appl. Phys. 115 (2014), 084907.
[38] N.K. Mukhopadhyay, A. Belger, P. Paufler, D.H. Kim, Nanoindentation studies on Cu–Ti–Zr–Ni–Si–Sn bulk metallic glasses, Mat. Sci. Eng. A. 449–451 (2007) 954–957.
[39] J. Gu, M. Song, S. Ni, S.F. Guo, Y.H. He, Effects of annealing on the hardness and elastic modulus of a Cu36Zr48Al8Ag8 bulk metallic glass, Mater. Des. 47 (2013) 706–710.
[40] J.W. Liu, Q.P. Cao, L.Y. Chen, X.D. Wang, J.Z. Jiang, Shear band evolution and hardness change in cold-rolled bulk metallic glasses, Acta Mater. 58 (2010) 4827–4840.
[41] Y.X. Ye, C.Z. Liu, H. Wang, T.G. Nieh, Friction and wear behavior of a single-phase equiatomic TiZrHfNb high-entropy alloy studied using a nanoscratch technique, Acta Mater. 147 (2018) 78–89.
[42] Y.Y. Zhao, Y.X. Ye, C.Z. Liu, R. Feng, K.F. Yao, T.G. Nieh, Tribological behavior of an amorphous Zr20Ti20Cu20Ni20Be20 high-entropy alloy studied using a nanoscratch technique, Intermetallics 113 (2019) 106561.
[43] F.P. Bowden, D. Tabor, Mechanism of metallic friction, Nature 150 (1942) 197–199.
[44] J.A. Greenwood, J.B.P. Williamson, Contact of nominally flat surfaces, P. Roy. Soc. A-Math. Phy. 295 (1966) 300–319.
[45] B.N.J. Persson, E. Tosatti, The effect of surface roughness on the adhesion of elastic solids, J. Chem. Phys. 115 (2001) 5597–5610.
[46] B.N. Persson, O. Albohr, U. Tartaglino, A.I. Volokitin, E. Tosatti, On the nature of surface roughness with application to contact mechanics, sealing, rubber friction and adhesion, J. Phys-Condens. Mat. 17 (2005) 1–62.
[47] U.D. Schwarz, O. Zwörner, P. Köster, R. Wiesendanger, Quantitative analysis of the frictional properties of solid materials at low loads. I. Carbon compounds, Phys. Rev. B 56 (1997) 6987–6996.
[48] D. Bandyopadhyay, P. Dinesh Sankar Reddy, A. Sharma, Electric field and van der Waals force induced instabilities in thin viscoelastic bilayers, Phys. Fluids 24 (2012), 074106.
[49] F.R. Poblete, Y. Zhu, Interfacial shear stress transfer at nanowire-polymer interfaces with van der Waals interactions and chemical bonding, J. Mech. Phys. Solid. 127 (2019) 191–207.
[50] Y. Li, S. Li, P. Bai, W. Jia, Q. Xu, Y. Meng, L. Ma, Y. Tian, Surface wettability effect on aqueous lubrication: van der Waals and hydration force competition induced adhesive friction, J. Colloid Interface Sci. 599 (2021) 667–675.
[51] A. Caron, D.V. Louzguine-Luzguin, R. Bennewitz, Structure vs chemistry: friction and wear of Pt-based metallic surfaces, ACS Appl. Mater. Interfaces 5 (2013) 11341–11347.
[52] C. Tangpatjaroen, D. Grierson, S. Shannon, J.E. Jakes, I. Szlufarska, Size dependence of nanoscale wear of silicon carbide, ACS Appl. Mater. Interfaces 9 (2017) 1929–1940.
[53] L. Dai, V. Sorkin, Y.W. Zhang, Effect of surface chemistry on the mechanisms and governing laws of friction and wear, ACS Appl. Mater. Interfaces 8 (2016) 8765–8786.
[54] J.N. Israelachvili, Van der Waals Forces between Particles and Surfaces, Intermolecular and Surface Forces, Academic. Press. Inc, San Diego, 2011, pp. 253–289.
[55] F.H. Zhang, B.B. Meng, Y.Q. Geng, Y. Zhang, Study on the machined depth when nanoscratching on 6H-SiC using Berkovich indenter: modelling and experimental study, Appl. Surf. Sci. 368 (2016) 449–455.
[56] S. Lafaye, True solution of the ploughing friction coefficient with elastic recovery in the case of a conical tip with a blunted spherical extremity, Wear 264 (2008) 550–554.
[57] S. Lafaye, M. Troyon, On the friction behaviour in nanoscratch testing, Wear 261 (2006) 905–913.
[58] M. Mishra, I. Szlufarska, Analytical model for plowing friction at nanoscale, Tribol. Lett. 45 (2011) 417–426.
[59] K.P. Marimuthu, J. Han, U. Jeong, K. Lee, H. Lee, Study on tribological characteristics of Zr-based BMG via nanoscratch techniques, Wear 486–487 (2021) 204067.
[60] J. Song, H. Shi, Z. Liao, S. Wang, Y. Liu, W. Liu, Z. Peng, Study on the nanomechanical and nanotribological behaviors of PEEK and CFRPEEK for biomedical applications, Polymers (Basel) 10 (2018) 142–156.
[61] Z.P. Wan, W. Wang, J.Y. Feng, L.J. Dong, S. Yang, Z.Y. Jiang, Effect of scratch direction on densification and crack initiation of optical glass BK7, Ceram. Int. 46 (2020) 16754–16762.
[62] S. Sawamura, R. Limbach, S. Wilhelmy, A. Koike, L. Wondraczek, Scratch-induced yielding and ductile fracture in silicate glasses probed by nanoindentation, J. Am. Ceram. Soc. 102 (2019) 7299–7311.
[63] C.A. Schuh, T. Hufnagel, U. Ramamurty, Mechanical behavior of amorphous alloys, Acta Mater. 55 (2007) 4067–4109.
[64] B.A. Sun, W.H. Wang, The fracture of bulk metallic glasses, Prog. Mater. Sci. 74 (2015) 211–307.
[65] F. Jiang, M.Q. Jiang, H.F. Wang, Y.L. Zhao, L. He, J. Sun, Shear transformation zone volume determining ductile–brittle transition of bulk metallic glasses, Acta Mater. 59 (2011) 2057–2068.
[66] A. Khmich, K. Sbiaai, A. Hasnaoui, Annealing effect on elastic and structural behavior of Tantalum monatomic metallic glass, Mater. Chem. Phys. 243 (2020).

[67] R.L. Narayan, P. Tandaiya, G.R. Garrett, M.D. Demetriou, U. Ramamurty, On the variability in fracture toughness of 'ductile' bulk metallic glasses, Scripta Mater. 102 (2015) 75–78.
[68] J.G. Lee, K.S. Sohn, S. Lee, N.J. Kim, C.P. Kim, In situ fracture observation and fracture toughness analysis of Zr-based bulk amorphous alloys, Mat. Sci. Eng. A. 464 (2007) 261–268.
[69] R.L. Narayan, D. Raut, U. Ramamurty, A quantitative connection between shear band mediated plasticity and fracture initiation toughness of metallic glasses, Acta Mater. 150 (2018) 69–77.